Ultrasound-transmission parameter imaging in a photoacoustic imager

J. Jose*[1], R. Willemink[2], S. Resink[1], T. Maalderink[1], J. C. G van Hespen[1], T G. van Leeuwen[1,3] and S. Manohar[1]

[1]MIRA Institute for Biomedical Technology and Technical Medicine, Biophysical Engineering Group, Faculty of Science and Technology, University of Twente, P.O. Box 217, 7500AE, Enschede, The Netherlands

[2]Signals and Systems Group University of Twente, P.O. Box 217, 7500 AE Enschede, The Netherlands.

[3] Biomedical Photonics, Academic Medical Center, University of Amsterdam, P. O. Box P.O. Box 22700, 1100 DE Amsterdam, The Netherlands

ABSTRACT

We present a 'hybrid' imaging system, which can image both optical absorption properties and acoustic transmission properties of an object in a two-dimensional slice using a computed tomography photoacoustic imager. The ultrasound transmission measurement method uses a strong absorber of light which is placed in the path of the light illuminating the sample. This acts as a source of ultrasound, whose interaction with the sample can be measured at the far-end of the sample using the same ultrasound detector used for photoacoustics. Such measurements are made at various angles around the sample in a computerized tomography approach. The ultrasound transients at the multi-element detector at all projections are analyzed for both times-of-arrival and amplitude. Using a fan-beam projection reconstruction algorithm we obtain hybrid images of optical absorption, speed-of-sound and acoustic attenuation. We validate the method on an appropriate phantom.

Keywords: (110.5120) Photoacoustic imaging, (110.7170) Ultrasound.

1. INTRODUCTION

Near-infrared photoacoustic imaging is enjoying much attention in the recent past [1] in the imaging of various pathological states related to vascular condition and function. Some important applications include breast cancer detection [2], skin cancer visualization [3] and small animal imaging [4]. The technique combines the advantages of optical imaging with those of ultrasound imaging. Optical imaging utilizes the high contrast exhibited by chromophores in the blood such as hemoglobin and oxy-hemoglobin, but suffers from poor resolution. Ultrasound imaging possesses higher resolutions due to the 2-3 orders lower scattering experienced compared with light and scalable with frequency, but is hampered by poor vascular contrast. The technique relies on irradiating the tissue surface with nanosecond pulses of visible or deeply penetrating near infrared (NIR) laser light. Optical absorption in the tissue causes a thermoelastic expansion, which produces broadband pulses (MHz) of acoustic energy. These pulses propagate to the tissue surface and are detected by an array of ultrasound transducers. By applying various reconstruction schemes with prior knowledge of the tissue-ultra sound transmission parameters, the acoustic signal can be backprojected in 3D to reconstruct a volumetric image of the internally distributed photoacoustic sources.One of the inputs for reconstruction algorithms, which are usually based on one or other form of backprojection algorithms [5] is the speed-of-sound of the medium through which the ultrasound propagates. This is used to translate the time-of-arrival of the ultrasound pulses into distance information in image space.

In most cases the speed-of-sound for tissue is not known precisely, and the assumption of an incorrect speed-of-sound (SOS) for reconstruction could lead to improper backprojections leading to compromised resolution and contrast.

* *J.Jithin@tnw.utwente.nl, phone +31 534893112, fax* +31 53 4891105

Novel Optical Instrumentation for Biomedical Applications IV,
edited by Christian D. Depeursinge, I. Alex Vitkin, Proc. of SPIE-OSA Biomedical Optics,
SPIE Vol. 7371, 73710S © 2009 SPIE-OSA · CCC code: 1605-7422/09/$18 · doi: 10.1117/12.831732

In this work we present the design and development of a curvilinear array based computed tomography photoacoustic imaging system optimized for "hybrid" imaging of both optical absorption properties and acoustic transmission properties of an object. A curvilinear array provides the most suitable configuration for tomographic imaging due to the matching to the cylindrical geometry. We begin with the short overview of instrument design and the detector characteristics followed by the validation results on chorioallantoic membrane (CAM) of the chicken embryo. Then we discuss the modifications which we made in the imager to provide the simultaneous imaging of ultrasound transmission parameters, followed by the validation on phantoms.

2. METHODS

2:1 Photoacoustic Computed Tomographic imager

The system consists of a Q-switched Nd:YAG laser, delivering 10 ns pulses at 532 nm to produce photoacoustic signals from the subject under investigation. The object is held stationary in an imaging tank with water. Figure 1 shows the schematic of the imager. The light beam enters through the top, is split along two paths, thus providing transmission mode and reflection mode illumination of the object in the center. However, in the measurements described here, the beam illuminates the object from the top through a set of beam expanders. The detector is placed orthogonal to the light illumination and it rotates around the object to perform the CT type measurement. The curvilinear detector array consists of 32 element ultrasonic transducers shaped to 85 degree of a circle of 40 mm radius. The center frequency of the array is 6.25 MHz with a reception bandwidth of greater than 80%. Individual elements feature an aspect ratio of 10 mm to 0.25 mm. These elements are arranged with an inter element spacing of 1.85 mm.

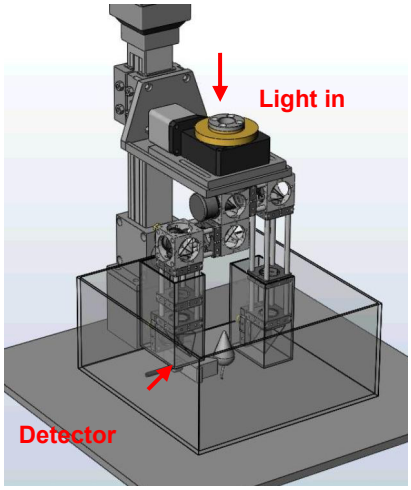

Figure 1(a): Schematic of the imager.

The photoacoustic signals from each element were individually amplified to 60 dB by using a 32 channel pulse-receiver system (Lecouer, Paris) with a sampling rate of 80 MHz. A modified acoustic back projection algorithm is used to reconstruct the images of the object [11].

The excited acoustic pressure ($p(r_0,t)$) from the source can be represented as

$$p(r_0,t) = \frac{\beta}{4\pi C_p c}\frac{\partial}{\partial t}\iint_{|r'-r_0|=ct}\frac{A(r')}{t}d^2r'$$

Where t is the time, β is the coefficient of volumetric thermal expansion, c is the sound speed, C_p is the specific heat, r' is the integral variable and A(r') is the spatial distribution of the electromagnetic absorption.

2.2. Chorioallantoic Membrane (CAM) Imaging

In our experiments, a 10 day old chick embryo is used. A window of 2.5 x 2.5 cm was cut from the shell, for the direct illumination of the light and the entire area is covered with a thin transparent foil to prevent the water leakage during the measurement. 2ml of phosphate buffer solution (PBS) was injected under the membrane to bulge out the blood vessels out of the window. A photograph of the CAM is shown in figure 2 (a). The sample was placed in the centre of the tank. Nine overlapping projections to cover 360 degrees were taken with fluence rate of 1.85 mJ/cm^2. Two slices of the membrane were taken with a spacing of 0.25 mm and the slice imaging was completed in 2 minutes.

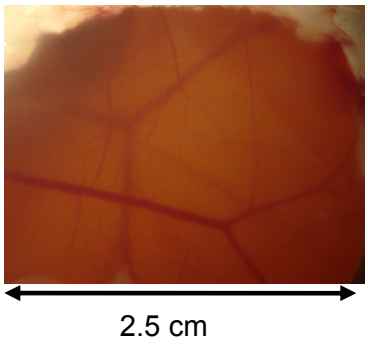

Figure 2(a): Photograph of the CAM.

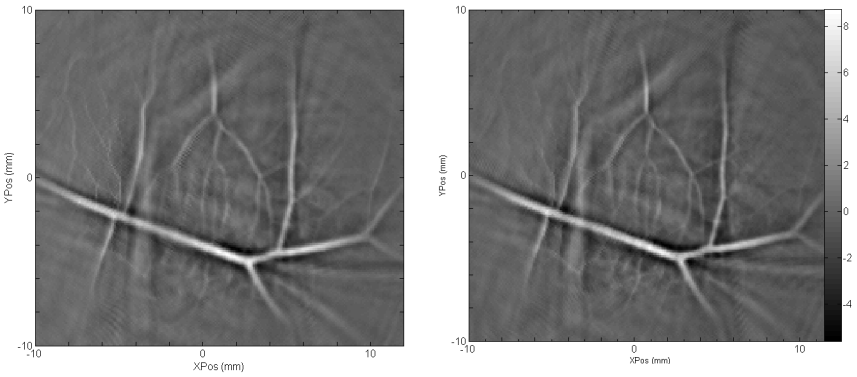

Figure 2(b) & 2(c) slices of the embryo with 1 mm separation.

Figure 2 (b) and (c) shows the reconstructed photoacoustic CT slice image of the Chorioallantoic membrane visualizing the blood vessels vasculature. It can be seen that the reconstructed photoacoustic images matches well with the distributions of vessels in the embryo and the branching of blood vessels up to the 3 order are clearly visible in the PA images. This was good validation study of the system with curvilinear array of ultrasound transducers. We are planning to continue this work with serial imaging of blood vessels development in the chick embryo.

3. MODIFICATION FOR ULTRASOUND TRANSMISSION PARAMETER IMAGING

For the ultrasound transmission parameter imaging, we use only one hardware appendage "a passive element", a strong absorber of light with a small cross section that is placed in the path of the laser light illuminating the object under photoacoustic examination [6]. Figure 3(a) shows the schematic of the method with the absorber being a carbon fiber and ultrasound transducers arranged antipodally with respect to the subject in water. Here for simplicity, we showed the curvilinear array as a linear array of Ultrasound transducers.

Ultrasound transients are generated in the extraneous absorber and in the object by the photoacoustic effect. The carbon fiber (250 μm) ensures that the acoustic waves fan out in the imaging plane but are collimated in the direction orthogonal to this plane. Ultrasound generated by this passive element interacts with the object and is collected on the far side by the transducer array. 30 projections around the object were performed with roughly 30 mJ of energy at 532 nm using 100 averages.

A reference measurement is also performed with the object removed. The signals from reference and object measurements are analyzed yielding times-of-arrival differences and acoustic attenuation differences compared with the reference. Obtaining projections around the object permits reconstruction of the cross-sectional map of the acoustic attenuation and speed-of-sound.

The ultrasound detector measures conventional photoacoustic signals from the object as well; the two sets of signals have different times-of-arrival (TOA) and are separated in the output trace of an element due to the finite distance between the carbon fiber and object. This technique provides a hybrid and more sophisticated way to image the ultrasound transmission parameter without any additional measurement to the conventional PA protocol.

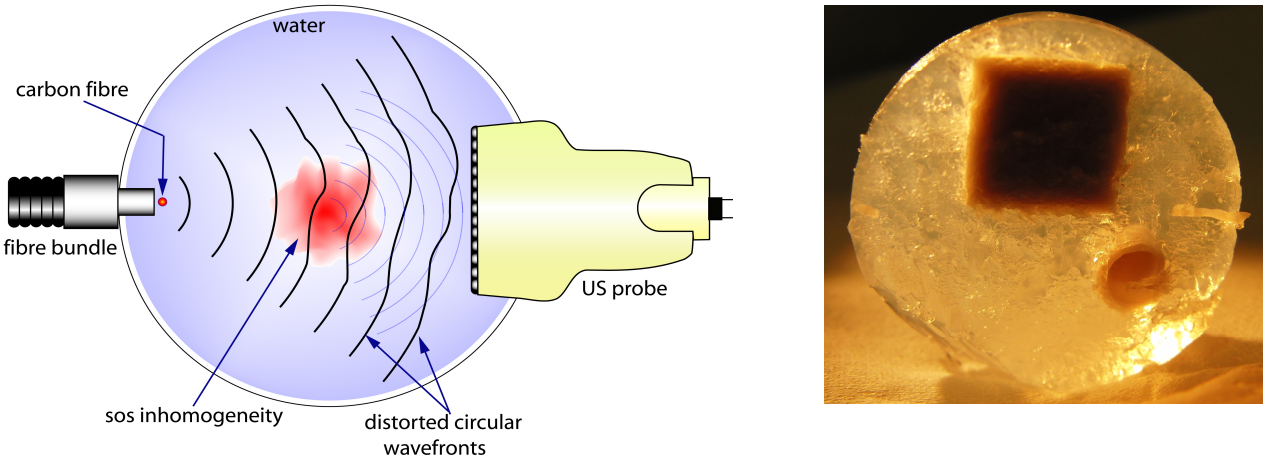

Figure 3(a): Schematic of the setup showing the concept of speed-of-sound/acoustic attenuation imaging using photoacoustics. The addition to the standard imager is a carbon-fiber introduced at the position of illumination. (b) Photograph of phantom. The phantom has two inhomogeneities with SOS and acoustic attenuation contrasts compared with background.

3.1. Phantoms

The phantom consisted of a 3% agar gel cylinder of 80 mm length and 26 mm diameter. This possessed 2 cavities: one with a square cross-section of 10 mm side and the other circular cross-section of 5 mm diameter. To prepare these acoustic inhomogeneities we follow the recipe suggested by Marinozzi *et al* [7].These cavities were filled with 3 % agar in a solution of 80:20 mixture of milk-water solution. 500µl of India ink ((μ_a = 1.4cm^{-1}) is added to the mixture to make these inhomogeneities as optically absorbing. We also placed an optically absorbing thread (Ø=120 µm) in a curly fashion at the left bottom of the phantom. (Not shown in the photograph). To characterize the inhomogeneities, we used the insertion technique [8] and obtained the values of speed of sound and acoustic attenuation as 1507m/s and 0.4 dB/cm/MHz respectively

3.2. Estimation of integrated speed-of-sound

The speed-of-sound may be calculated in the time domain or the frequency domain. In a first approximation, the time-of-arrival (TOA) of the ultrasound transient at a detector element is the line integral of the inverse of the SOS distribution encountered by a ray traversing the path from source to the detector. The normalized TOA at element n is:

$$\Delta t_n = \int_{l(\phi,n)} \frac{ds}{v_s} - \int_{l(\phi,n)} \frac{ds}{v_w}$$

Where l is the ray-path defined by rotation angle Φ and detector position n, $v_w(v_s)$ are the acoustic velocities in water (sample). The normalized TOA is obtained by a cross-correlation between the signals at every element position when the object is present, with their corresponding signals when the object has been retracted. In such a case the time-of-arrival (TOA) difference between sample and water, at an element position for a certain angle is obtained. The group velocity may then be calculated as:

$$v_s = \frac{v_w}{1 + \frac{v_w \Delta t_n}{l(\phi, n)}}$$

However, in tissue due to frequency dependent attenuation, dispersion will be present, which causes various phase components of the broadband pulse to travel at different velocities. This could lead in cases to distortion in the signal shapes making a time-domain analysis by cross-correlation inaccurate.
In such cases, the phase spectral method may be used which is performed in the frequency domain. Here the FFTs of the sample and water signal are obtained; the phases are subtracted from each other to yield the phase difference of the frequency component in the sample and that in water. From this the phase velocities may be calculated as:

$$v_s(\omega) = \frac{v_w}{1 + \frac{v_w \Delta\phi(\omega)}{l(\phi, n)}}$$

For the phantoms that we use, the differences between the cross-correlation method and the phase-spectral method at the central frequency of the transducer are negligible since the phantoms are not expected to have any considerable dispersion. However, the phase-spectral method is more appropriate for tissue and it is advisable to use the frequency domain method for estimating SOS.

3.3. Estimation of integrated acoustic attenuation

In a similar way to SOS, the acoustic attenuation may be calculated in the time domain or in the frequency domain. In the first approximation, neglecting interface losses and under the assumption of negligible water attenuation, a ratio of amplitudes with and without the object in water, leads to the acoustic attenuation:

$$\alpha_s(\mathrm{dB}) = 20\log_{10}\left\{\frac{A_s(t)}{A_w(t)}\right\}$$

In the log-spectral method, the amplitudes of the spectral components are treated as:

$$\alpha_s(\omega) = 20\log_{10}\left\{\left|\frac{A_s(\omega)}{A_w(\omega)}\right|\right\}\ \mathrm{dB}$$

In a more realistic scenario the attenuation is frequency dependent. Attenuation of most materials follows a frequency power law [9]

$$\alpha_s(\omega) = \alpha_0\left|\omega^y\right|$$

Where α_0 is the material dependent attenuation constant and y is a material dependent parameter that ranges between 0 and 2. Specifically, in a realistic scenario in soft tissue, the parameter $y = 1$. In this case, estimation of the attenuation constant can be done in the frequency domain by fitting the data to the expected frequency dependent attenuation function. In such a case errors due to interface losses are minimized since these are expected to be constant and not dependent on frequency.

3.4. Reconstruction of Acoustic Property Distributions

Once projections of both the integrated parameters for estimating SOS and acoustic attenuation have been obtained, the acoustic property maps have to be reconstructed. The unknown acoustic property distribution is discretized by sampling over a grid with uniform spacing. Each sample point on the grid represents the value of the acoustic property distribution at that location, off- grid points are interpolated via bilinear interpolation. The projection measurements can be expressed as a linear combination of a number of sample points. To construct this linear combination, a line is traced through the grid connecting the source and detector. At regular intervals a sample is taken. Bilinear interpolation is then used to express the sample as a linear combination of samples. For each projection angle and each detector element such a projection measurement is available, resulting in a linear system:

$$Hx = z\,,$$

Where the matrix H is formed by tracing along the projection lines and the vector z represents all individual projection measurements. Since the construction of the matrix H is based on tracing the projection lines we have to know the geometry of the complete experimental setup, i.e. the positions of the source, the detectors and the center of rotation. All of these geometrical parameters are known roughly in advance, but are fine-tuned using the water measurement as a

calibration [10]. Once the projection matrix H is constructed, the reconstruction of the acoustic property distribution is done by solving for x. Since the matrix H is large and sparse, the linear system can efficiently be solved with the LSQR algorithm. Both the attenuation and speed of sound distribution can be reconstructed using the above outlined algorithm. In case of the attenuation distribution, we use the integrated attenuation measurements as input and directly obtain a distribution of the attenuation constant. In case of the speed of sound distribution, the delay time between reference and object measurements is used as input resulting in an output image of the relative delay time per unit distance.

4. RESULTS AND DISCUSSIONS

The images of speed-of-sound, acoustic attenuation and optical absorption from the ultrasound parameter imaging are shown in figure 4. The gross features of the phantom can be recognized in the 3 images.

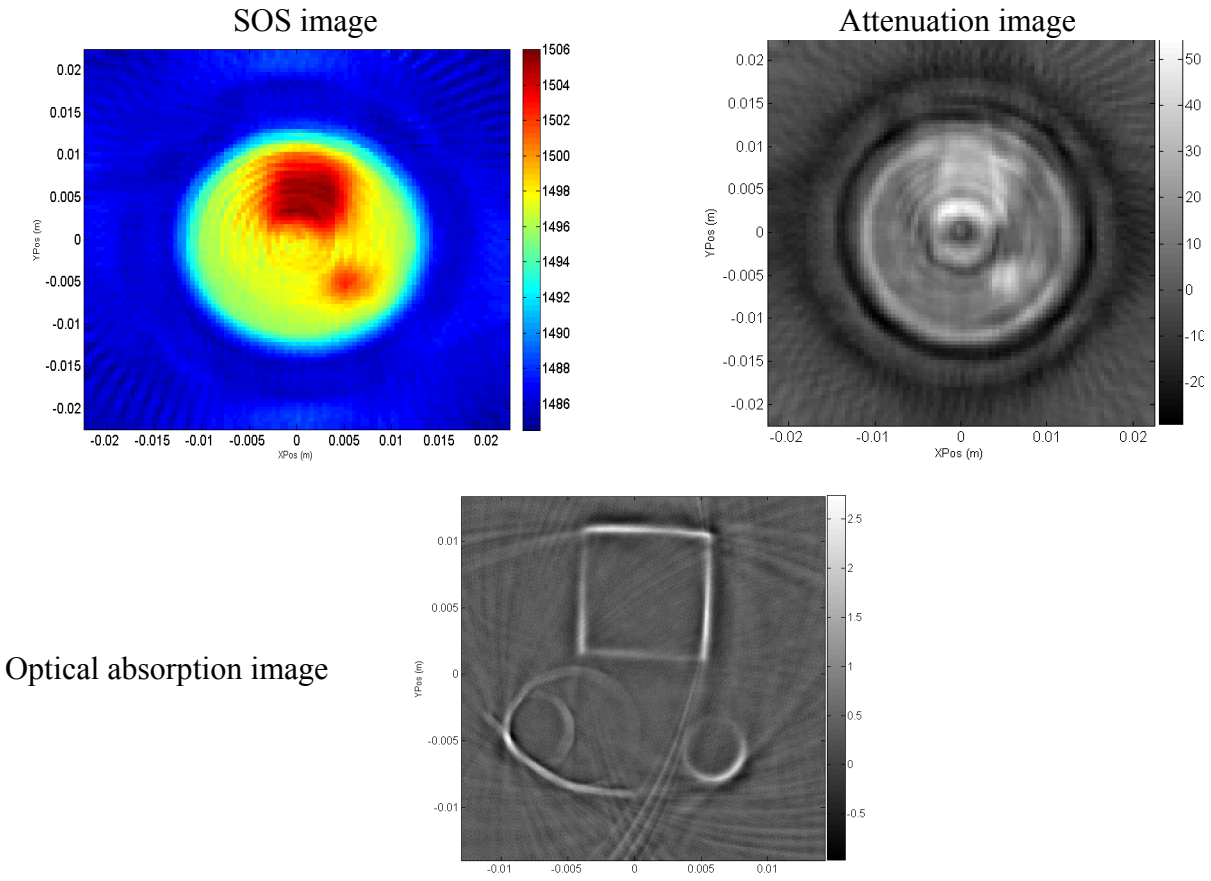

Figure 4: Results of the reconstruction of acoustic property distributions and conventional photoacoustic mapping of the phantom.

The values of the speed of sound (SOS) map shows faithful reconstruction, compared with the actual values designed into the phantoms, but the edges of the inhomogeneities are smeared out. During the experiment the phantom was immersed in the water at temperature of 22 degree Celsius. In the reconstructed SOS image, the surrounding water has a speed of sound of 1488 m/s. This is in accordance with the literature [11]. On the other hand the acoustic attenuation is reconstructed the inhomogeneities with refraction artifacts. The photoacoustic image shows the curly thread, but it shows

only the outer surface of the inhomogeneities since these are highly absorbing due to the high content of optical absorption preventing further light penetration into the structures.

CONCLUSIONS

The methodology and the analysis are successful in imaging three parameters of the phantom. Such an approach permits not only functional information from conventional photoacoustics to be extracted but also anatomic and morphological information from ultrasound parameter depiction. Even the SOS image shows faithful reconstruction of the actual values, the acoustic actuation image shows ring artifacts and a mismatch with the expected values. The program for the reconstruction of acoustic attenuation is being investigated at the moment and some solutions have been identified. Future work will concentrate on obtaining better measurements without the noise which has plagued the resent experimental data. Further, when the technical and the programming difficulties have been resolved, we will make images of more complicated phantoms and finally combined with of small animals such as mice.

ACKNOWLEDGEMENTS

This research is funded by the Institute of Biomedical Technology (BMTI) of the University of Twente via the PRESMITT program; and by SenterNovem through the project IPD067771 in the theme IOP Photonic Devices.

S.M. thanks the Netherlands Organization of Scientific Research NWO and the Technology Foundation STW for a personal grant in the Vernieuwingsimpuls program.

REFERENCES

[1] M. Xu, L. V. Wang, "Photoacoustic imaging in biomedicine", Rev. Sci. Instrum. 77, 04110 (2006)
[2] S. Manohar, S. R., Vaartjes, J. C. G. van Hespen, F. van den Engh, J. M. Klaase., W. Steenbergen, , T. G. Van Leeuwen, "Initial results of near-infrared imaging of the symptomatic breast using Photoacoustics," Opt. Exp. 15, 12277 (2007)
[3] J. T. Oh, M. L. Li, H. F. Zhang, K. Maslov, G. Stoica, L. V. Wang, "Three-dimensional imaging of skin melanoma in vivo by dual wavelength photoacoustic microscopy," J. Biomed. Opt. 11, 34032 (2006)
[4] Wang X, Pang Y, Ku G, Xie X, Stoica G and Wang L V 2003 Noninvasive laser-induced photoacoustic tomography for structural and functional in vivo imaging of the brain Nature Biotechnol. **21** 803–6X.Wang et al,"Noninvasive laser-induced photoacoustic tomography for structural and functional in vivo image of the brain"Nat.Biotechnol, 21,803 (2003).
[5] S. J. Norton, M. Linzer, "Ultrasonic reflectivity tomography: reconstruction with circular transducer arrays," Ultrason. Imaging 1, 154 (1979)
[6] S. Manohar, R. G. H. Willemink, F. van der Heijden, C. H. Slump, and T. G. vanLeeuwen," Concomitant speed-of-sound tomography in photoacoustic imaging" Appl. Phys. Lett. 91, 131911 (2007)
[7] F. marinozzi, D. Piras and F.Bini, "Spectral Analysis of Backscattered Ultrasound Field from Hydroxyapatite granules"Advances in Medical, Signal and Information Processing, 2008. MEDSIP 2008. 4th IET International Conference on , vol., no., pp.1-4, 14-16 July 2008.
[8] J.C Bamber 1997 "Acoustical Characterisation of Biological Media", Encyclopedia of Acoustics 4th edn (New York: Wiley)
[9] K. R. Waters, J. Mobley, G. J. Miller, ""Causality-imposed (Kramers-Kronig) relationships between attenuation and dispersion", IEEE Trans. Ultrason, Ferro Freq Control, 52, 822 (2005).

[10] G. H. Willemink, S. Manohar, Y. Purwar, F. Van der Heijden, C. H. Slump, T. G. Van Leeuwen, "Imaging of acoustic attenuation and speed of sound maps using photoacoustic measurements," Proc. SPIE 6920, pp. 692013 (2008)

[11] Lubbers and Graaf, Technical Guides - Speed of Sound in Pure Water. http://resource.npl.co.uk/acoustics/techguides/soundpurewater/content.html, 1998.